International Journal of Multiphysics
Volume 18, No. 3, 2024
ISSN: 1750-9548

Deep machine learning approaches for evaluating the Comprehensive Strength of Ultra-high Performance Concrete

Saadia. A. Sahii

Southern Technical University, Basrah, Iraq

* Corresponding author's e-mail: Saadiya.abdulsada@stu.edu.iq

Abstract - Ultra-high performance Concrete (UHPC) C.S.S. is determined by the kind, characteristics, and composition of its material ingredients. Using intelligent techniques, such as the ANN, to create a prediction framework that adjusts within an implementation dataset is often necessary to empirically capture this link. However, scientists cannot quantitatively describe its contents because of its opaque character. This research uses two deep machine learning approaches to determine the crucial material components that impact the Artificial Neural Network: Neural Interpretation Diagrams (N.I.D.s) and Sequential Feature Selections (S.F.S.). 110 Ultra-High Performance Concrete C.S.S. tests with different material amounts were combined into a database to train the ANN. Thus, Four material components were chosen: cement, fly ash, silica fume, and water. After that, the ANN was used with these material components to make more accurate predictions than those made by the model that included all eight material constituents (r2 = 21.5% and NMSE = 0.035) (r2 = 80.1% and 0.012). Ultimately, parametric research was carried out, and a nonlinear regression framework was created depending on the four chosen material elements. The use of Artificial Neural Networks with Sequential Feature Selections and Neural Interpretation Diagrams was shown to significantly increase the model's accuracy and provide insightful information about the ANN CS forecasts for various Ultra-High Performance Concrete combinations.

Keywords: Neural Interpretation Diagrams; Compressive strength; UHPC; deep learning.

1. Introduction

ANNs are ML algorithms widely used in many domains to assess predicted outcomes that closely match experiment results. However, an experiment might include many parameters in a thorough test matrix, most showing minimal assistance in the test results. Computer researchers were forced to create new selection techniques depending on data-driven frameworks to quickly reduce the dimensionality of the I/P matrix and find the most crucial independent variables. Soft computing techniques are becoming more and more necessary to forecast engineering frameworks, materials, and components precisely. Artificial neural networks are an admired soft computing model successfully implemented in various engineering spheres. ANNs are often used to expect and estimate matters related to pattern recognition, image processing, classification, and optimization. It encouraged scientists to suggest Artificial Neural Network frameworks and resolve various civil engineering issues.

Additionally, several studies show broad applicability in artificial neural network behavioral modeling of concrete structural elements. Utilizing different ANN frameworks to direct predictive-dependent difficulties with steel, concrete, and composite construction elements is currently a more popular research area. Most issues about concrete's new and hardened possessions were effectively directed via ANN modeling based on gathered experimental data. Furthermore, using ANN models to estimate the C.S.S. of concrete has been a constant research focus. It encouraged analysts to use ANNs to evaluate the C.S.S. of recycled, light-weight, and normal-weight concrete. Utilizing diverse ML approaches, other studies looked at several prediction frameworks to detect the C.S.S. of higher-performance concrete. Later, the development of UHPC called for more Artificial

Neural Network modeling to be developed to make behavioral predictions. Although ANN models have been effectively created to replicate UHPC performance accurately, these "black-box" models supply less information about the inner workings of ANN computations. Thus, the next step in furthering the campaign should be rectifying this inequality using intelligent algorithms to evaluate UHPC mix performance and providing a mathematical justification. The use of optimization approaches during the Artificial Neural Network training step to iteratively choose the parameters that affect the model's accuracy has shown promising results in deep machine learning. The selected parameters may then be used in the Artificial Neural Network or diverse, innovative regression methods to increment the prediction framework's accuracy when comprehending the fundamental physical occurrence. This study presents a deep learning (DL) approach depending on an artificial neural network that uses DL methods to pinpoint the crucial variables that affect how accurately the C.S.S. (C.S.S.) of UHPC is predicted. The exhibited UHPC compressive strength (C.S.S.) tests provide an extensive library of experimental findings with several parameters. Subsequently, an array of ANNs with varying topologies was used repeatedly to produce a final model reliably. Then, using S.F.S. and N.I.D., this model is used to methodically choose the material components that affect the model's estimates of UHPC compressive strength. Lastly, an analytical model is created using the previously chosen material elements, and parametric tests are carried out to examine their correlations with the C.S.S. of UHPC.

2. The Foreground of Artificial Neural Network and UHPC

Structural engineers demonstrated the endurance, flexibility, and C.S.S. of heavily loaded reinforced concrete structures because of UHPC's advancement. For the past 40 years, various scientists have been examining the mechanical action of UHPC and its implementation. According to these studies, UHPC typically shows a C.S.S. that falls between 160 MPa and 850 MPa. A higher dose of cement (up to 850 kg/m^3), a lesser water/binder ratio (< 0.30), a higher-range water-decreasing blend, fine powders (squeezed quartzite and nano-SiO_2), and steel or polyethylene fibers are the ingredients needed to produce a material with such a high compressive strength. Additional researchers sought to create cost-effective and sustainable methods by lessening the cement and SiO_2 fume content and comprising these with sand and fly ash.

Nevertheless, most of the previously listed mixes seldom estimate the intensity of UHPC and need a significant amount of resource exhaustion and batch testing. Therefore, to forecast C.S.S. values quickly and precisely, an analytical framework that is a basis of the elements of UHPC must be developed. Using statistical mixture designs and backpropagation neural network (BPNN) in forecasting the necessary UHPC performance was examined by (Harith I.K. et al. 2024). Their goal was to use statistical mixture design and BPNN to estimate the C.S.S. and stability of UHPC utilizing two well-defined curing methods, namely steam and wet curing. Depending on the design matrix of the statistical blend pattern, 53 concrete specimens were generated, and the mixture's constituents were used as the BPNN framework's self-sufficient parameters. According to the findings, BPNN outperformed statistical mixture design in its ability to forecast C.S.S. and slump flow. Despite their data's complexity, inadequacy, and incoherence, (Zhang H. et al. 2024) utilized Artificial Neural Network to estimate the perfect mixture % of cement, SiO_2, superplasticizer, water, fine aggregate, and coarse aggregation for HPC. Their framework displayed a massive link between the observed actual and anticipated estimates, allowing an ANN model to be used to estimate the ideal combination. To check the connection between the C.S.S. and the ratio of element amounts to restore age for various aqueous lime cement concrete blends, (Haghsheno, H. et al. 2024) constructed a series of artificial neural network models. The models' correlation coefficients, which differed from 92.3 to 97.5%, show they were fruitful in estimating the C.S.S. of various concrete mixtures. Despite the excellent accuracy of the formerly suggested Artificial Neural Network models, reducing the input parameters would simplify the ANN structures and improve the computational efficiency of their models. As a result, scientists created reliable methods for revealing the characteristics of the ANN model by figuring out which independent factors had the most influence on the ANN's accuracy.

3. Literature Review

One of the developed techniques is feature selection, wherein the algorithm sorts the feature sub-sets according to an established performance measure (i.e., error/performance) that counts otherwise in each additional feature subset to find the features that significantly provide the estimation model. This methodical selection procedure

enhances the model's accuracy and precision while facilitating a more profound comprehension of data processing. There exist two primary feature selection methods: the wrapper technique that gauges the effectiveness of the independent variables by looking at the performance of the regression/classification model and the filter method that emphasizes the inherent qualities of the independent variables as determined by basic statistics. The wrapper approach, the S.F.S. algorithm, was the main focus of this work. (Sakshi, Bhatia, M.P.S. et al. 2024) Choose the most important characteristics of human motion recognition using the Sequential Feature Selection paradigm inside the Markov Blanket, a different ML approach. The outcome was a quick reduction in the number of characteristics, which enhanced the algorithm's capacity to demonstrate higher recognition accuracy than conventional techniques. To address groundwater quality issues (Kumar P. et al. 2024) also used S.F.S., in which 20 parameters were extracted from an extensive database. The study used four different ML methods with a sequential selection of features and identified the underlying characteristics affecting the effectiveness of each machine learning method. For this reason, the Rainforest machine learning framework used in S.F.S. was affected encouraging. U. et al., 2024) used a neural interpretation diagram (N.I.D.) approach to investigate habitat selection by marsh-nesting bird species in different areas. The method was integrated into ANN models to efficiently extract essential parameters from the entire data set and visually explore the relative consequences of each habitat variable related to the classification process for C.S.S. of UHPC by On the Implementation of Sequential Feature Selection and N.I.D. in BPNN. Machine learning algorithms selected controls and final important attributes that improved the performance of the BPNN system by analyzing eight features from 110 UHPC CS tests collected from an extensive database. Furthermore, selected attributes were used and included in the conventional Abram procedure for accurate C.S.S. analysis. Finally, each parameter was analyzed using selected attributes to evaluate the effect of material properties behavior on the C.S.S. of UHPC.

4. Modeling methodology

Four methodical procedures formed the basis of the investigation: gathering data, confirming the BPNN, carrying out S.F.S. (Khanh, P. T. et al. 2024) and N.I.D., and analyzing certain aspects. This method is shown in Fig. 1 as a flowchart where a reliable and accurate prediction model might be created. The instructions for training the data iteratively until a backpropagation neural network (Ashisha G. R. et al. 2023) formation, which may provide predictions that are both accurate and consistent, are explained in the 1st and 2nd boxes (I/P Data and Design/Validate backpropagation neural network Framework). The use of DL approaches (S.F.S. and N.I.D.s) to methodically choose the elemental components that affect the precision of the backpropagation neural network estimations in the training stage is shown in the 3rd box (Execute SFS/NID). The last rectangle, "Analyze Selected Material Constituents," requires a thorough parametric analysis highlighting the connection between the changes in material amounts in various UHPC mixtures and the compressive strength.

Table 1 lists the familiar components of UHPC mixes employed in various experimental studies and the statistical data (mean, median, standard deviation, maximum, minimum, and related code names).

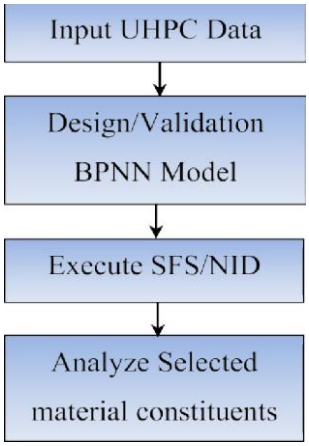

Figure 1: Deep machine learning method flowchart.

They are using a trial-and-error method to get an exact answer. ANN (Andrushia, A. D. et al. 2023) models come in feed-forward and feed-backward models. For the feed-forward to create predictions, the artificial neural network (ANN) model must have an updated or taught network using the back-propagating (B.P.P.) approach. The feed-backward model employs the genuine response variables to calculate the error or cost between them while attempting to estimate the predictor variables. The method then modifies the weights so that the neural network eventually converges on the best precise answer. Because of this, the backpropagation feed-forward multilayer perceptron (Veeraiah, V. et al. 2024) is mainly utilized in many technical contexts. A typical artificial neural network (ANN) architecture consists of wires, I/P neurons, hidden neurons (Chandan, R. R. et al., 2023), bias units, and O/P neurons. The hidden neurons map the weights variables utilizing user-defined activation functions, the bias units direct the O/P function's shift (rising or descending), and the wires constitute arbitrarily created matrices termed weights, which operate the function's slope. The I/P neurons contain every parameter as a vector (I/P by the user). Eq. (1) displays a vectorized representation of the complex blend throughout the scrutiny interval in an isolated-hidden layered system.

$$B(Y) = k(\alpha^m Y + c^m) \qquad (1)$$

In $B(Y)$ the vector representation of predictions, k (Y) is the activation function, a vector comprising the bias units in layer k, and Y represents the input parameters as a matrix. α^m It is a matrix comprising arbitrarily produced weights per layer m (beginning with the hidden layer). Every row was altered in a specific field utilizing a user-defined activation function before making the final output. The sigmoid function, as shown in Eq. (2), was used in this investigation.

$$f(y) = \frac{1}{1+e^{-f_i}} \qquad (2)$$

Furthermore, every C.S.S. level was assessed 28 days after the casting process. Fig. 2 displays a layered figure of the frequency distributions for every material ingredient our research looked at.

4.1. ANN

An ANN is an ML paradigm that simulates the learning processes of the human brain mathematically by examining various experiences recorded by the neurons and The Levenberg-Marquardt approach, a repetitive approach that shows the local minima of a multivariate function shown as the sum of squares of nonlinear real-valued functions is utilized by the B.P.P. methodology as a minimization cost strategy. The Levenberg-

Marquardt approach employs the Gauss-Newton (Mondal, D. et al., 2023) and the Gradient Descent methods to aid solution convergence. The iterative method is summed up in an algebraic matrix form

$$L^M L\partial j = L^M e \qquad (3)$$

L is the Jacobian matrix $\frac{\partial f(j)}{\partial(j)}$, and e is the error or expenditure $(J(\omega) = \| \frac{1}{2P}\sum_{p=1}^{P}(X(S^m) - R^m)^2 \|)$.

The solution is denoted by δ_j when the column space $J\delta_j$ is orthogonal to the solution found by J. For example, modifying or dampening the components in $J^{M.J.}$ While T J calculates δP, the cost ε is subject to variation. After that, the value of ω is modified by using Equation (4), and the value of B(Y) is recalculated by utilizing Equation (1). This technique is repeated until the value of ε lowers, which ultimately decreases the damping rate as the result gradually converges.

$$\omega_1 = \omega_0 + \partial_j \qquad (4)$$

Where ω_1 and ω_0 are the weights that have been changed and the weights that were initially used, respectively.

Table 1 Span of I/P parameters used in training, validation, and testing.

Sign			Mathematical calculations				
Variable (Kg/m^3)	Encoded		Minimum	Highest	Mean	Median	SD
Cement	C		379	1650	880.5	779	330.3
SiO_2 fume	SI		0	371.82	193	197	95.8
Flyash	FA		0	449	35	0	73.6
Sand	SA		0	1885	979	1108	514.5
SteelFiber	SF		0	480	40	0	75.9
QuartzPowder	QP		0	760	37.8	0	123.8
Water	W		110	335.6	198.2	186.2	55.2
Admixture	A		0	187	32.8	29.2	29.3
fc (MPa)	fc		96	243	154.4	148.5	32.6

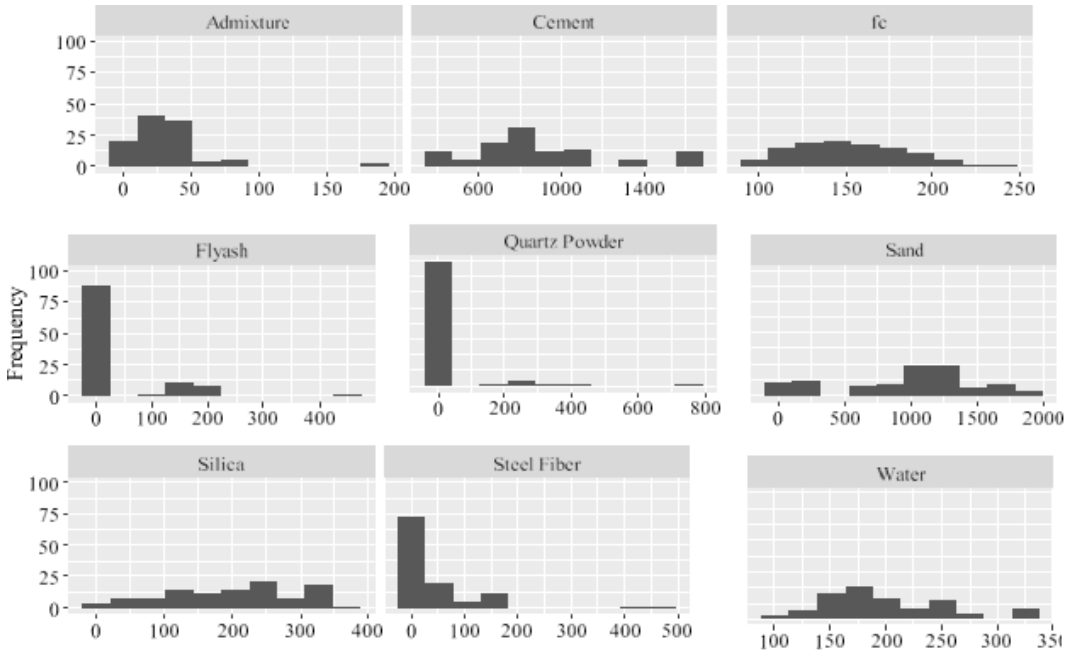

Fig 2. Experimental data frequency distribution

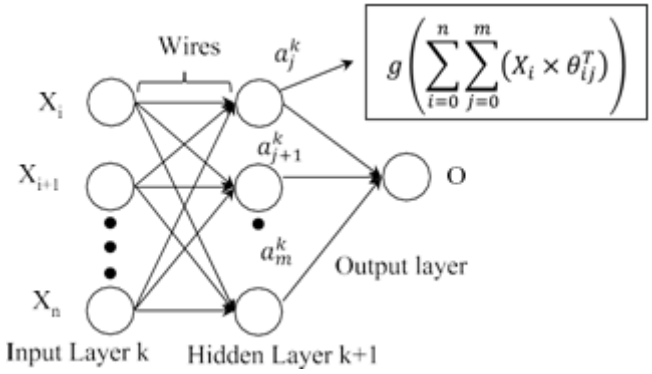

Fig 3 Architecture of ANN

The illustration of an ANN with an I/P layer, a single hidden layer, and one O/P layer is shown in Fig. 3. The neuron and layer numbers are denoted by superscripts and subscripts, respectively. In the end, the subscripts *i* and *n* represent the number of neurons in the I/P layer k, which are individual and total, respectively. Until and unless n neurons are supplied into the BPNN (Mall, P. K. et al. 2023) formation, every I/P neuron, *Xi*, holds an independent parameter. X_{i+1} holds the successive column. Similarly, in a haphazard hidden layer *k+1*, every hidden neuron, a^{k+1}, gets weighted matrix products from every neuron, *Xi*, through the wires linking the I/P and hidden layers. The subscripts *j* and *m* indicate the isolated and cumulative quantity of neurons, respectively. These wires, which have weights ω, convert the mapped sum products onto the adjacent layers.

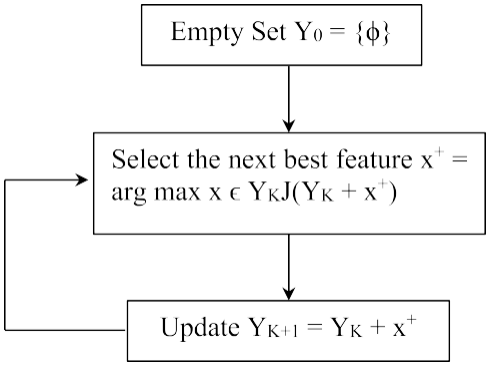

Fig 4 Forward selection technique

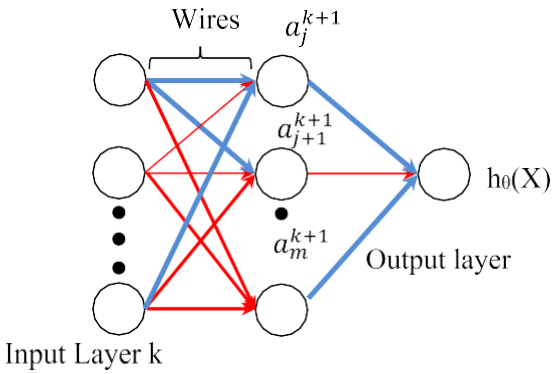

Fig 5 The NID

4.2 SFS

By choosing a subset of the observed features and creating a more straightforward prediction model, feature selection lowers the dimension of the data. The algorithm uses the goal function to track criteria while choosing features, and the search technique, which is the method the ML search algorithm has employed in multiple research, makes up this machine learning algorithm. (Akhiat, Y. et al. 2024) The S.F.S. is a function initialized in evaluating a predictive model and adds variables to the framework one after the other until the objective function is sufficiently changed. The study employed the NMSE as the goal function and the S.F.S. search algorithm within a BPNN. The algorithm that S.F.S. applies during a selection is depicted in Fig. 4.

4.3 NID

An artificial neural network (ANN) structure called a neural interpretation diagram (N.I.D.) shows how important an independent variable is about a response variable based on the weights' signs and magnitudes. During the analysis stage, the algorithm breaks down the weights for every input node before a list of weights is

kept in a matrix. One value is then derived for every I/P variable, which expresses the link with the response variable in the framework after the matrix has been scaled concerning all other input variables and is equal to each input node. Users can use this information to determine the kind of association the network promotes and to find out which I/P variables are muted by the weights and unimportant. The network with input parameters positively correlated with the network—that is, more relevant—observes the contrary. An instance of an N.I.D. illustration with a single output unit and one hidden layer is shown in Fig. 5. A red line represents a negative association of the I/P variable with the network, which reduces the prediction model's accuracy. On the other hand, solid blue lines show the favorable combination from 1 neuron to the next neuron(s), with bold lines indicating more significant associations.

4.4 Nonlinear Regression

The theoretical and experimental results' cost or standard error is minimal. To perform these calculations, the standard error is used to iteratively pick the proper parameters, which may be exponents or multiplicative coefficients. The fundamental error is expressed as a function of the parameters in Eq. (5), where n denotes the quantity of data points in the dataset, Cov(x, x) is the x^{th} diagonal element in the covariance matrix, and S.S.R. is the cumulative squared residuals.

$$N_{error}(X_i) = \sqrt{(\frac{SSM}{m-1}) XCov(x,x)} \quad (5)$$

As a result, executing S.F.S. and N.I.D. will minimize the independent parameters and enhance convergence in the evaluation. The user computes the parameters, and incorrect guesses may cause the framework to diverge from the real outcome. As demonstrated in Eq. (6), Abram's formula (Le, BA. et al. 2024) was employed as the mathematical framework for the nonlinear regression analysis since it may be used to estimate the C.S.S. of 7 and 28-day-old concrete. The IBM SPSS 23 software program was used to do nonlinear regression.

$$f_m = BXY^{-C} \quad (6)$$

B and C are the regression coefficients, and Y is the water-to-binder ratio.

5. ANN modeling to forecast UHPC CSANN design

5.1 ANN Design

BPNN was utilized in this work to determine the most pertinent attributes and to create predictions. Using MATLAB, the Levenberg-Marquardt minimization approach was used to build the BPNN. The training parameters included 10−7, 0.001, total epochs, learning rate, and the minimal gradient. The BPNN framework, where the UHPC elements were normalized and expressed as a ratio of the material ingredient to cement, was trained and tested using 112 examinations with eight material elements. This reduced any extreme outliers in the sample and helped prevent significant swings in the results. Table 2 displays the C.S.S. values (highest and most minor) and the normalized parameters range (highest and least) expressed as a % of cement.

5.2 Validation of ANN

Within the BPNN, two different validation methodologies should be used: numerical solver validation and overfitting validation. With each B.P.P. analysis, the procedure of numerical solver verification involves increasing the number of neurons sequentially. The error is vector-stored and shown against the number of neurons during each run. The over-fitting check prevents the BPNN from learning to read a particular range of inputs and can be used to predict outcomes using a freshly gathered database. Levenberg-Marquardt, the BPNN's numerical solver, was initially tested by testing a random subset of neurons and calculating the model's performance for each neuron utilizing the NMSE as an indicator. The increment in this investigation was one neuron to fifteen neurons, with ten analyses of the model performed on each neuron.

Table 2

Training and testing normalized data.				
Sign			Span	
Variable	Symbols		Minimum	Maximum
Cement	C		O	1
SiO_2 fume	SI		0	0.342
Fly ash	F.A.A.		0	1.02
Sand	S		0	3.9
Steel Fiber	S.F.F.		0	0.452
Quartz Powder	Q.P.P.		0	0.946
Water	W		0.1045	0.523
Admixture	A		0	0.291
f'c (MPa)	fc		96	235

Consequently, 10 NMSE estimates were assessed and recorded in a matrix for every neuron that had been trained. The mean and 96% confidence gap were computed for every column vector (neuron) and displayed as a dotted line and a darkened area, respectively, about the quantity of neuron(s). The data was randomly divided into three sets, with 70% referring to the training set, 15% referring to the validation set, and 15% going to the testing set during the implementation of the initial verification phase. When the two procedures were combined, the verification strategies mirrored a k-fold cross-validation strategy, in which the I/P parameters of the model were arbitrarily split into isolated groups and again trained until the finest-achieving ANN was created. The confirmed ANN architecture is depicted in Fig. 6. The neurons with the letters I and H succeeded by a number represent the I/P and concealed neurons, respectively, with the related quantity of units, and the neurons with the alphabets B and O succeeded by numbers represent the bias and O/P units.

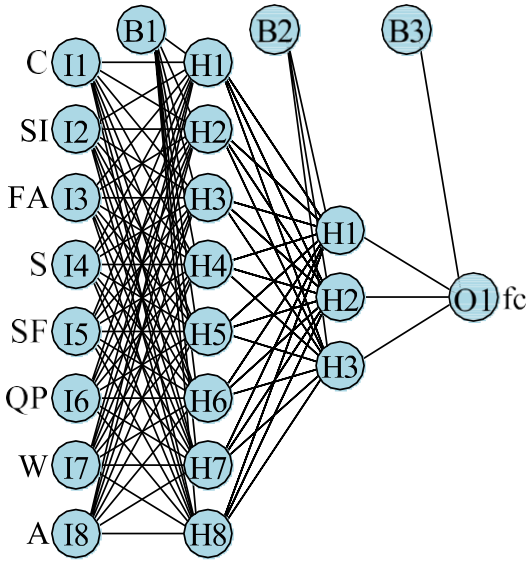

Fig 6 Architecture of ANN

6. Methods of variable significance S.F.S. implementation

6.1 Implementation of S.F.S.

Using a BPNN, the S.F.S. approach was run on 200 occasions to collect every attainable combination of self-sufficient attributes. A bar plot illustrating the proportion of attributes utilized in the 200 trials is displayed in Fig. 8. A criterion of 20% was set as the lesser constraint for choosing the variables that had the most significant assistance based on the outcomes of these attempts and the most prevalent connection found in the research. The bar chart's form, which revealed a pattern when looking at the tiny percentage differences between the four factors that had contributed more than 20% of trials, was the basis for the 20% selection. As a result, the most pertinent elements in the prediction model were determined to be the four variables: cement, SiO_2 fume, fly ash, and H_2O. Preparation methods and curing schedules significantly improve the performance of UHPC. This has also prompted ongoing research into the impact of material constituents on UHPC's compressive strength. Additionally, researchers have carried out experimental studies employing these precise material components to track the C.S.S. performance of UHPC individually.

6.2 Implementation of S.F.S.

To visually check the features during the study, the chosen parameters in the S.F.S. approach were plotted within the validated ANN using the N.I.D.

Table 3 Mathematical computations utilizing ANN before and following SFS/NID.

Statistical Computations	Before selecting	After selecting
r^2	0.216	0.802
Normalized Mean Square Error	0.036	0.013

Table 4 Coefficients of L.S.G.

Regression Coefficients	Coefficient estimates	r^2	Normalized Mean Square Error
B	94	0.717	0.0646
A	0.36		

As mentioned in Fig. 5, a positive alliance with the reply is depicted with a bold blue line, and an opposing partnership with the reply is shown with a red line. This is because the weights determine the relative consequence of the data prepared in the network. R, statistical programming software, was used to plot the N.I.D. Utilizing the former validated ANN framework, the N.I.D. diagram is displayed in Fig. 8. It is evident from the analysis that C, SI, F.A.A., and W all exhibit robust positive correlations; S.I.I. and W, in particular, show the most substantial positive relationships with their surrounding hidden units, resembling the bar plot in Figure 7. The width, color, and quantity of blue wires in Fig. 9—the majority of which had optimistic, significant weighted estimates that reflect their dominant properties in the BPNN framework—were used to measure this visually. Because the material elements chosen in this section match those selected in the preceding paragraph, there has been consistency in identifying features inside a predictive model using both S.F.S. and N.I.D.

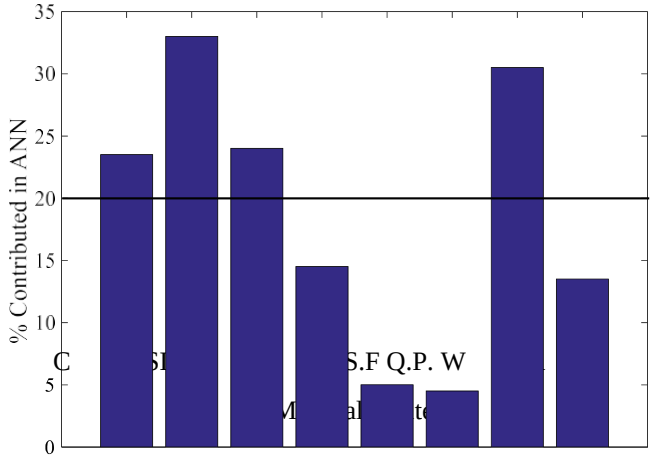

Fig 7 A bar plot illustrating the proportion of characteristics that were responsible for the model's creation

7. Result and Discussion

ANN outcomes

Consequently, the trained ANN that employed the chosen features demonstrated better agreement with the implemented data than the ANN before the selection. The statistical measurements for both situations are displayed in Table 3, where the coefficient of numerous determinations (r^2) was utilized to quantify the difference between the mean of the experimental results and the data from the prediction model. The total difference between the expected and experimental findings was measured using the NMSE. The results showed that the NMSE was 0.035 before and after selection, and the r2 value was 21.5% and 80.1%, respectively, before and after selection. Additionally, correlation graphs were created for both trained ANN models between the experimental and projected results, as illustrated in Fig. 10, where the dotted lines indicate the % difference (16%) from the perfect fit and the red line indicates an ideal fit for the data. Therefore, the ANN with the chosen features could predict 81.2 percent of the time within the 15% threshold, while the ANN with all the characteristics could only predict 62% within a similar threshold. It concluded that the framework with the chosen characteristics performed better than the model with every feature.
The chosen-to-implemented composite strength ratio for both ANN frameworks is shown in Fig. 11, where the framework with the chosen features performed better than the ANN having all features (65.4%), with a more significant % of estimates (89.1%) falling between 0.9 and 1.3.

7.2. A model built with nonlinear regression analysis

Equation (6), which gives Abram's formula, was revised by enlarging X to a water-to-binder formation, as provided by Equation (7). This was done using IBM SPSS 23, and a nonlinear regression analysis was started. W, C, SI, and F.A. material constituents were expressed in kg/m^3. Consequently, Table 4 presents the results of the regression coefficient together with the statistical calculations. The NSME and r^2 values for the suggested model were 0.0645 and 71.6%, respectively.

$$f_d = BX\left(\frac{X}{(D+SI+FA)}\right)^{-A} \qquad (7)$$

Figure 11 provides a summary of the performance of the suggested framework and the connection between the projected and implemented data for C.S. The Artificial Neural Network framework that was evolved here could predict the concrete strength with a higher level of accuracy. However, the accuracy of the Artificial Neural Network prediction framework and its restriction in estimating concrete strength is limited by the boundaries of the I/P parameters that were utilized in training the Artificial Neural Network. These boundaries are the highest and least values of the nine parameters shown in Table 1. For I/P values that fall beyond the boundary values domain, it is impossible to guarantee that the anticipated concrete strength will be accurate and secure.

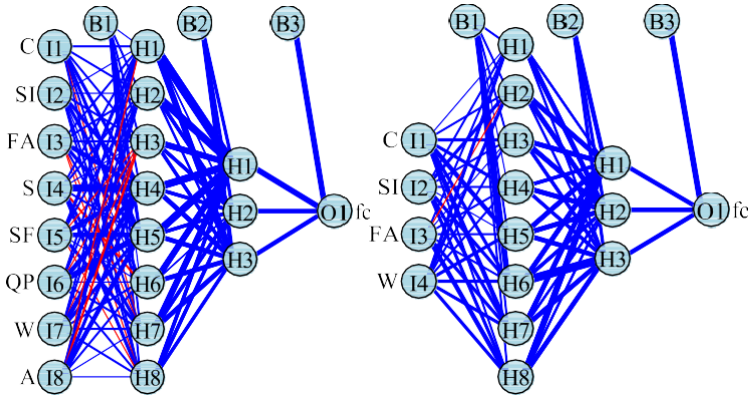

(a) Before S.F.S. (b) After S.F.S.

Fig 9 N.I.D. participation

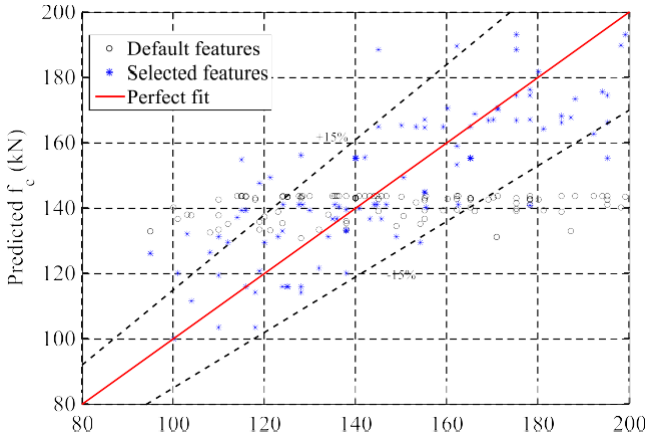

Fig 10 Percentage of expected vs. implemented deviance

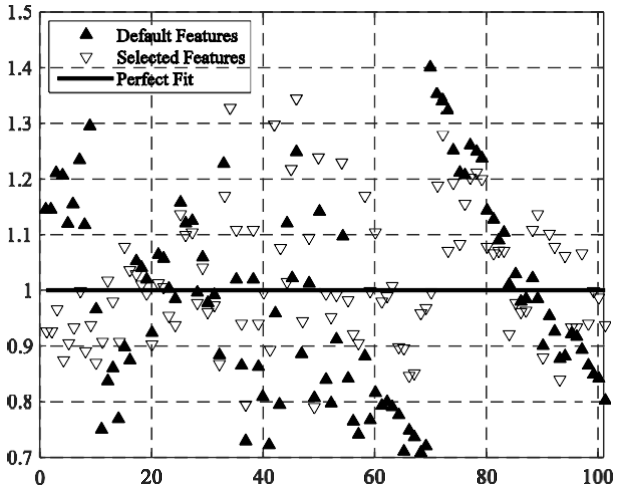

Fig 11 Ratios of the two ANN models, both projected and experimental

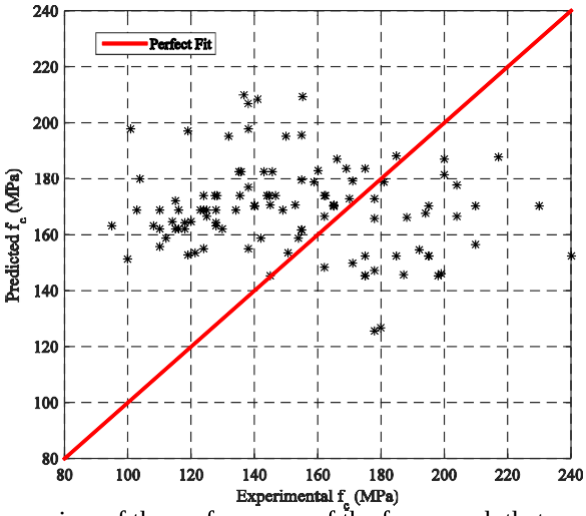

Fig 12 An overview of the performance of the framework that was suggested

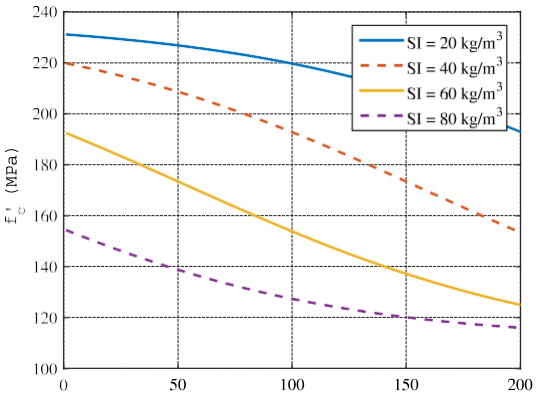

(a) Cement = 800 kg/m^3, Water = 100 kg/m^3 =

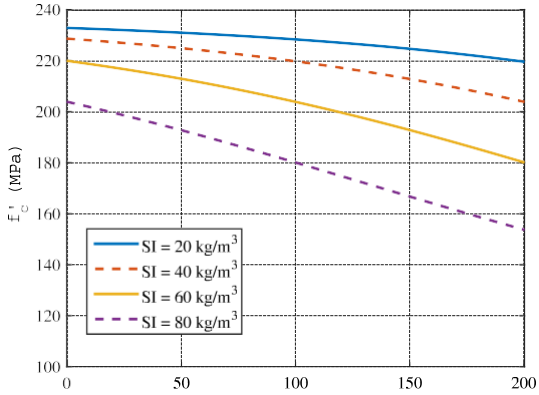

(b) Cement = 1202 Kg/m^3, H_2O 151 Kg/m^3

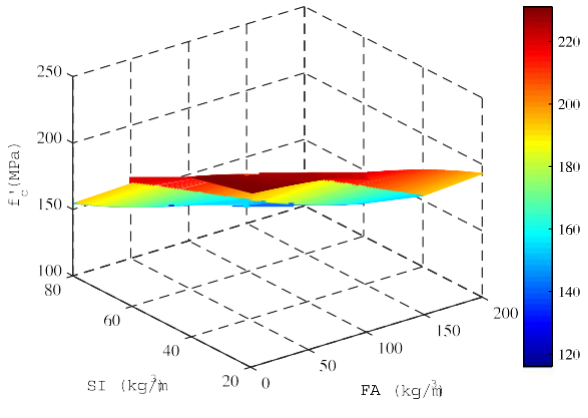

(c)Cement = 802 Kg/m^3, H_2O = 102 Kg/m^3

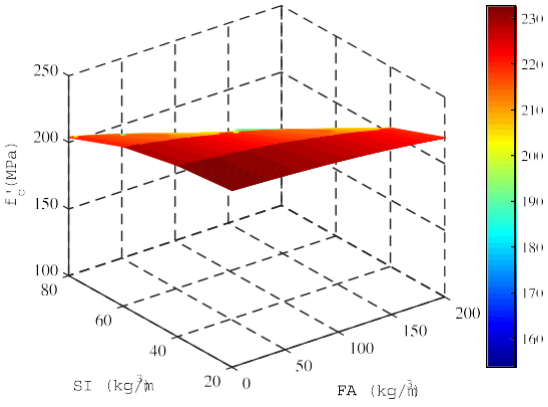

(d) Cement = 1202 Kg/m^3, H_2O = 150 Kg/m^3

Fig 13 Impact of fly ash on the presence of different amounts of SiO_2 fume

Table 5 The parametric research is summarized below.

The study of parameters	Constant ratios	Changing parameters (Kg/m^3)
In the presence of specific concentrations of silica fume, the effect of fly ash	The ratio of H_2O to cement equals 13.5%	Volatile ash (0–202) 20, 40, 60, and 80 percent silica fume
The role of SiO_2 fumes on specific amounts of fly ash is to be chosen.	The ratio of water to cement is 12.5%.	Silica fume (ranging from 0 to 200) 40, 80, 120, and 160 grams of fly ash
The impact of water on specific amounts of fly ash was calculated.	25% is the ratio of cement to silica fume.	(100–350) water 40, 80, 120, and 160 grams of fly ash
Influence of water on the concentration of silica fume in specific concentrations	25 percent cement to fly ash ratio	(100–350) water 20, 40, 60, and 80 percent silica fume

8. Sensitivity analyses and parametric research

Given that the suggested artificial neural network (ANN) model could accurately forecast outcomes consistent with the implemented data, a parametric analysis was carried out to examine the impact of the chosen parameters on the C.S. of ultra-high-performance concrete. Plots were produced with some independent parameters kept constant and others altered within their helpful range of values. The final ANN framework may be put into the MATLAB computing environment to perform the parametric research. It is crucial to observe that before beginning the parametric analysis, the material elements can be standardized against cement, as described in the module "Design of ANN."

8.1 Planning of the Parametric Research Project

The pattern and allocation of the data were examined so that reasonable ranges were enforced inside the higher and lower boundaries of the I/P parameters in the artificial neural network before the parametric analysis was carried out. Table 1 has further details about these statistical metrics. Every implementation (row) in the data displayed a basic connection regarding the associated material components during data collection. For example, an increment in cement was correlated with an increment in fly ash, SiO_2 fume, and H_2O; this indicates that these material elements had a specific ratio. As a result, the kept material components had their ratios unchanged via every parametric research while creating the matrix. The investigation's parametric research, which involved fixing certain ratios and varying the others for each study, is summarized in Table 5. Impact of fly ash at different levels of silica fume Fly ash's impact on UHPC's C.S. is depicted in Fig. 13 at various silica fume concentrations (20, 40, 60, and 82 kg/m^3) and a fixed H_2O/cement ratio of 13.1%. Figures 13(a) and (b) showed that every single curve showed an inverse connection between the C.S. response for all amounts of silica fume and the fly ash (independent variable). Furthermore, the mixtures depicted in Figures 13(a) and (b) demonstrated their highest C.S. values if fly ash and SiO_2 fume levels were kept at 0.1 kg/m^3 and 21 kg/m^3, respectively. The action occurred despite the significant variation in cement quantity. With the constant addition of the curve's C.S. decreased somewhat; as a result, the mechanical performance of UHPC was impaired by the inclusion of both fly ash and SiO_2 fume. On the other hand, if the amounts of cement and water were raised by 49% sans altering the water and cement ratio, an increment in C.S. was noted. For instance, as shown in Fig. 13(a), the UHPC blend showed a significant drop in C.S. from 236.9 MPa to 156.7 MPa at 0.1 kg/m^3 of fly ash when SiO_2 fume ranged between 21 kg/m^3 and 81 kg/m^3. However, as depicted in Fig. 13(b), the mix displayed less of a drop in C.S. at 1 kg/m^3 of fly ash, going from 236.1 to 210.4 MPa when the same additives of SiO_2 fume were added. Consequently, the tendency for a UHPC mix's C.S. to decrease due to a rise in fly ash and SiO_2 fume is suppressed when the amounts of cement and water increase. Additionally, when silica fume was raised, there was a noticeable shift in the behavior of both curves. As seen in Fig. 13(a), there was an upward concave curve at a SiO_2 fume of 80 kg/m^3 and a downward concave curve at a SiO_2 fume of 20 kg/m^3. Fig. 13(b) illustrates that

every curve is downward concave, even though SiO_2 fume changed from 21 kg/m^3 to 81 kg/m^3. This is because the amounts of cement and water were increased to 1205 kg/m^3 and 155 kg/m^3, respectively. This demonstrated that, in comparison to the blend with lower amounts of cement and water, depicted in Fig. 13(a), the existence of SiO_2 fume at large amounts of cement and water provides a downward concave shape (Fig. 13(b)), allowing the UHPC to employ better C.S. In conclusion, the following findings can be noted: (a) UHPC's C.S. falls as fly ash content rises; (b) the highest C.S. is reached at 1 kg/m^3 of fly ash; (c) the inclusion of each cement and water causes the C.S. to shift within the inverse profiles and (d) lower tendencies of even with drastic variations in the amounts of silica fume, growing inflection points were visible when cement and water were added in greater amounts. Surface plots of the previously indicated 2D plots in generic contour plots are displayed in Figs. 13(c) and (d). The impact of SiO_2 fume on the C.S. of UHPC is depicted in Fig. 14 at fixed water/cement ratios of 12.6% and specific fly ash quantities of 40, 80, 120, and 160 kg/m3. There are two kinds of correlations shown in Fig. 14. When silica fume was added, there was a dramatic increment in C.S. as illustrated in Fig. 14(a), which also displayed a parabolic drop in consolidated strength until and unless a local least value was attained. On the other hand, Fig. 14(b) showed an inverse parabolic profile up until a local minima estimate, beyond which there is a small rise in C.S. due to the silica fume injection. Both figures reveal a distinct underlying variation in slope and horizontal shift characteristics. For instance, the blend in Fig. 14(a) displayed a greater difference in C.S., 237.4 MPa to 236.3 MPa, despite the same mixtures in the amounts of fly ash. The mixture of fly ash (41 - 161 kg/m^3) to the blend attained the highest C.S. estimates, which ranged from 235.5 MPa to 226.2 MPa at 0 kg/m^3 silica fume. As demonstrated in Fig. 14(a) and (b), it is evident that the rise in silica fume caused the C.S. of the UHPC to drop following a local minimum estimate was attained, at which point its consequence was reverted to enhance the compressive strength. The minimum C.S. values showed a shift in a horizontal direction along with this event; however, the minimum C.S. remained relatively unchanged with the addition of cement and water. However, as Fig. 14(b) illustrates, the mix of cement and H_2O led to a decrease in slope as silica fume increased. This suggested that the mix in question is more resilient than the one in Fig. 14(a), where the silica fume mixture causes a sharp decline in compressive strength. The quantity of SiO_2 fume needed to conclude at the same, at least roughly C.S., was likewise impacted by this decrease in slope. In conclusion, the succeeding conclusions may be drawn: (a) the C.S. of UHPC exhibits a semi-inverse parabolic curve and minimizes with the increment in SiO_2 fume to arrive at a particular local minimum; (b) the largest C.S. is obtained at 0 kg/m^3 despite a 51% increment in cement and H_2O; (c) the amount of fly ash does not affect the C.S. at certain silica fume values; (d) the mixture of fly ash brought about the least compressive estimates to show horizontal shifts; (e) the increment in cement and H_2O influenced the slope of the profiles where the C.S. estimates didn't significantly differ with the mixture of fly ash. Surface plots of the previously indicated two-dimensional plots in generalized contour plots are displayed in Fig. 14(c) and (d).Impact of water at different fly ash concentrations. The impact of water on the C.S. of UHPC is depicted in Fig. 15 for constant cement/silica fume ratios of 25% and at specific fly ash quantities of 40, 80, 120, and 160 kg/m^3. The curves in Figures 15(a) and (b) show a positive parabolic connection between the C.S. and water. As the amounts of water increased, both values showed comparatively little variation in compressive strength. Curves showing a maximum and a minimum are shown in Fig. 15(a).

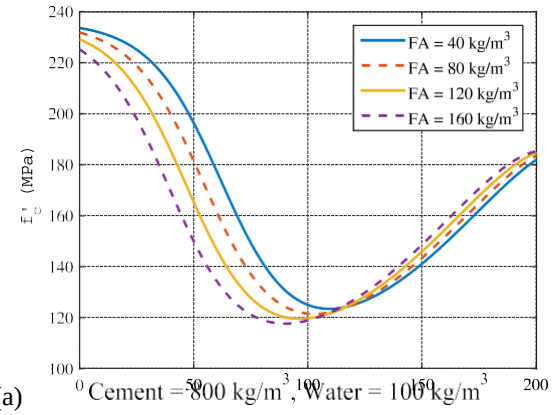

(a)

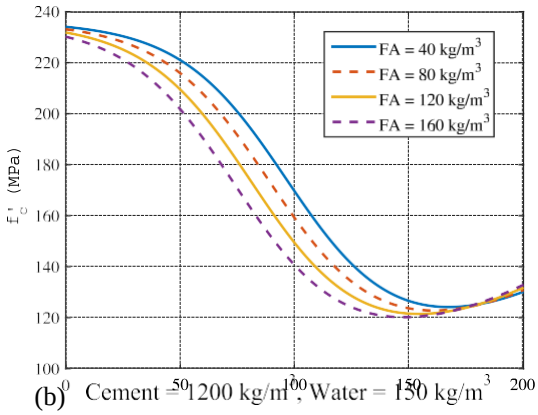

(b)

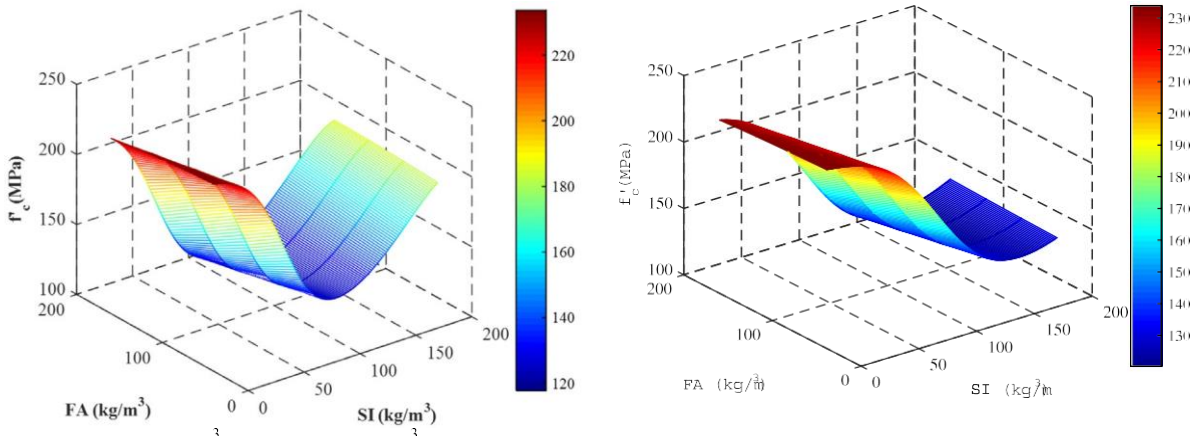

(c) Cement = 800 kg/m^3, Water = 100 kg/m^3 (d) Cement = 1200 kg/m^3, Water = 150 kg/m^3

Fig 14 A comparison of the effects of silica fume on different amounts of fly ash

The maximum C.S. was measured at 126 kg/m^3 of water and the least at 264.4 kg/m^3 of water, ranging from 135 to 186 MPa. When the amount of water surpasses the threshold corresponding to the minimal values, the impact of fly ash on C.S. is more noticeable. In contrast, curves in Fig. 15(b) showed a larger C.S. of 184–187 MPa, attained at 176 kg/m^3 of water. Fly ash has a minor beneficial influence on C.S. between 100 and 151 kg/m^3 of water, but its effect diminishes between 160 and 268 kg/m^3 of water and becomes more pronounced above 300 kg/m^3 of H_2O, as Fig. 15(a) illustrates. Likewise, a 50% increase in cement and silica fume moved the largest C.S. but did not affect it. In addition, the mix curves in Figure 15(b) needed more water to achieve the same largest C.S. as Figure 15(a). To sum up, the subsequent findings may be noted: Fly ash has a minimal impact on C.S. across a wide range of water quantities; (b) fly ash has a more significant effect on C.S. at large water quantities for lower cement and silica fume quantities; (c) An increase in cement and silica fume quantities has no consequence on the maximum compressive strength. Surface plots of the previously stated 2D plots in generic contour plots are displayed in Fig. 15(c) and (d).

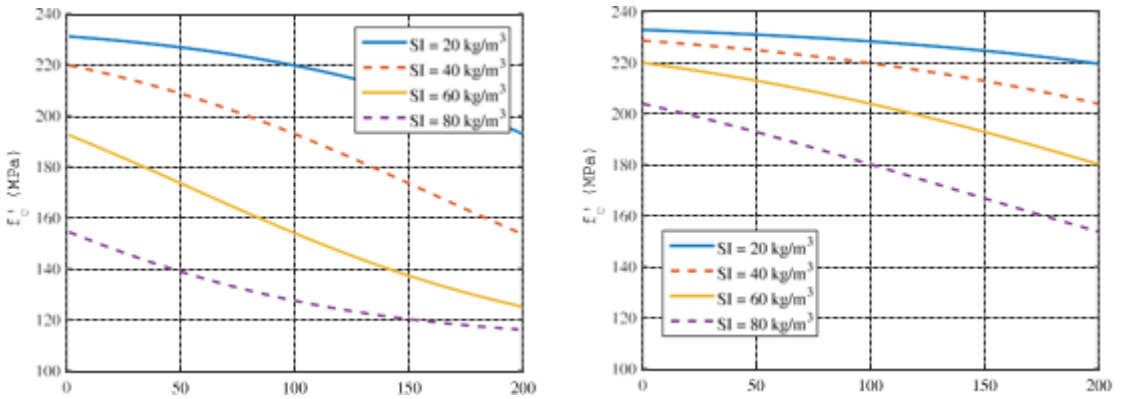

(a) Cement = 800 kg/m^3, Silica Fume = 200 kg/m^3 (b) Cement = 1200 kg/m^3, Silica Fume = 300 kg/m^3

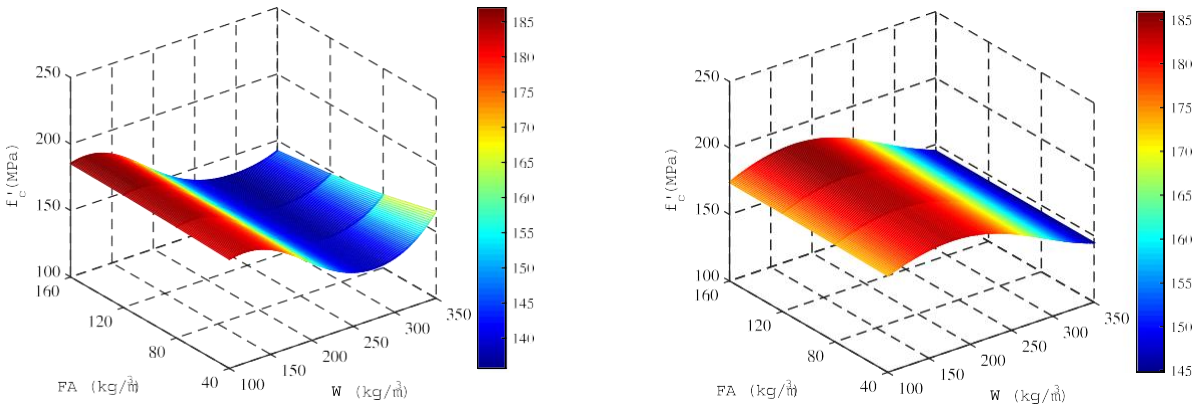

(c) Cement = 800 kg/m^3, Silica Fume = 200 kg/m^3 (d) Cement = 1200 kg/m^3, Silica Fume = 300 kg/m^3

Fig 15 Impact of water in different concentrations of silica fume

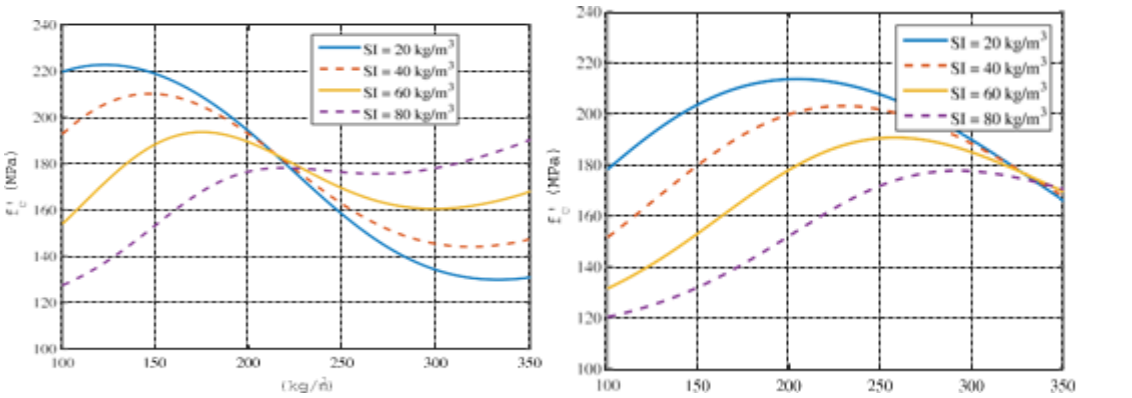

(a) Cement = 800 kg/m^3, Fly ash = 200 kg/m^3 (b) Cement = 1200 kg/m^3, Fly ash = 300 kg/m^3

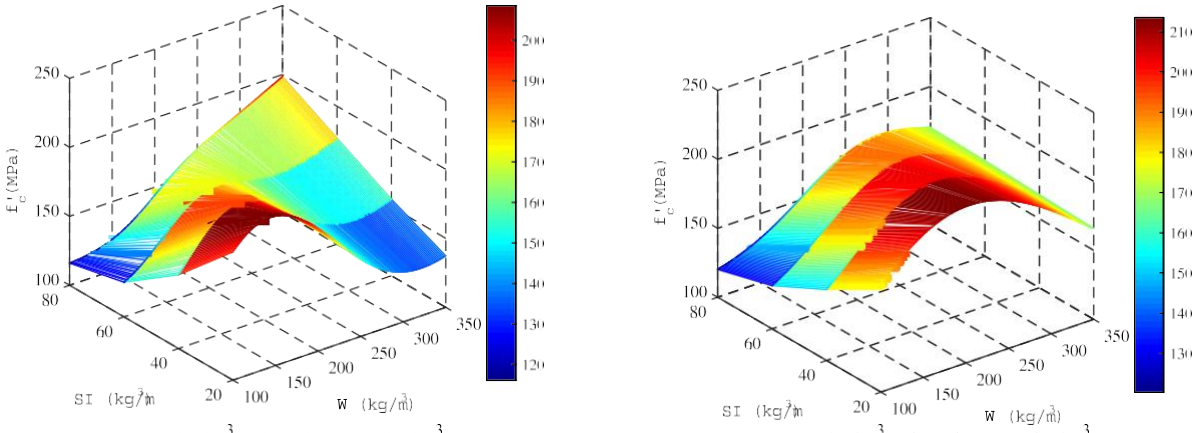

(c) Cement = 800 kg/m^3, Fly ash = 200 kg/m^3 (d) Cement = 1200 kg/m^3, Fly ash = 300 kg/m^3

Fig 16 Result of water on the presence of silica fume at varied concentrations

The impact of water on the C.S. of UHPC is depicted in Fig. 16 at fixed fly ash/cement ratios of 26% and specific silica fume concentrations of 20, 40, 60, and 80 kg/m^3. According to Fig. 16(a), UHPC's C.S. rises with

an increment in water volume up to a predetermined C.S. for a certain amount of silica fume. When silica fume levels rise from 20 to 60 kg/m^3, there are noticeable decreases in compressive strength. Nevertheless, the framework shows a plateau in C.S. when silica fume levels rise, requiring more water to enable a discernible increment in compressive strength. For example, at a water amount of 158 kg/m^3, the mixture containing the least amount of silica fume (41 kg/m^3) reaches a maximum C.S. of 224 MPa, while the mix containing the most amount of SiO_2 fume (161 kg/m^3) reaches the least C.S. of 177 MPa. 200 kg/m^3, as Figure 16(a) illustrates. All mixes with varying amounts of silica fume reached a similar C.S. of about 176 MPa at about 200 kg/m3 of water. At that point, the behavior changed, showing that mixes with higher amounts of silica fume had compressive strengths that increased steadily as the amount of water increased. While the behavior in Fig. 16(b) is comparable to that in Fig. 16(a), more water was required for the mixtures to achieve their largest compressive strength. Like the blends in Fig. 16(a), all the mixes in Fig. 16(b) met at a similar C.S. of 173 MPa but with a higher water content of 340 kg/m^3. To sum up, the succeeding findings may be noted: (a) The C.S. curves displayed negative vertical shifts that resembled the inverse connection depicted in Fig. 14(a) and (b). The mixture of fly ash sequentially caused (b) the curves to shift horizontally in the amounts of SiO_2 fume; (c) the curves with varying amounts of silica fume showed varying highest C.S. calculations at varying amounts of water; and (d) curves with huge amounts of SiO_2 fume needed extra water amounts to extend their highest C.S. Surface plots of the previously stated 2D plots in generic contour plots are displayed in Fig. 16(c) and (d).

9. Conclusion

The paper aims to use artificial neural networks (ANN) and the most crucial concrete mix factors to estimate the C.S. of UHPC. The inquiry was divided into four main phases: (1) using the S.F.S. and NID ML tools to find and choose the best essential features or parameters; (2) utilizing BPNN to analyze the features that were chosen; (3) utilizing nonlinear regression to modify and calibrate Abram's classical framework; and (4) conducting a sensitivity analysis for investigating the consequence of every feature selection on the characteristics and action of UHPC. The following are the study's results: By combining BPNN with S.F.S. and N.I.D., the database's dimensionality was quickly reduced, which made it easier for the prediction framework to assess C.S. estimates. Compared to the framework that included all eight parameters (r2~21.5%; NMSE = 0.035), the BPNN framework that included the four features that were chosen was able to predict the results more correctly (r2 80.1%; NMSE = 0.012)—moreover, contrasted to just 62% of values predicted utilizing every eight parameters, 81.2% of values predicted utilizing the four parameters that were chosen fall within the 15% deviation boundary limit. Nonlinear regression was used to alter Abram's classical model, and a new model was put forth. It produced results with an NMSE of 0.0645 and an r^2 of 71.6%, similar to the experimental results. It has been noted that UHPC's maximum C.S. was attained in the absence of silica fume, and its least C.S. was attained by adding more silica fume until a specific concentration was reached.

Additionally, it was noted that the C.S. of UHPC decreased as fly ash was added. This decline was accompanied by a horizontal displacement, showing that the silica fume mixture didn't affect the compressive strength. A parabolic connection was seen when the C.S. was plotted against the water constituent. In essence, the mix needs more water to enable a noticeable improvement in C.S. at a particular level of fly ash and incremented amounts of SiO_2 fume. When fly ash levels increase, this relationship moves to the right, indicating higher water demands for the extra binders (fly ash and SiO_2 fume). The study's produced curves can be used to understand the fundamental links between the design mix material elements and the C.S. of UHPC and anticipate the C.S. of UHPC mixes. It is crucial to stress that there are restrictions on the accuracy of the ANN framework created in the paper despite its accuracy. Whether or not the I/P parameters fall into the range of the relevant boundary values utilized to train the ANN framework has a significant impact on these restrictions.

References

1. Andrushia, A. D., Neebha, T. M., Patricia, A. T., Sagayam, K. M., Pramanik, S., Capsule Network based Disease Classification for VitisVinifera Leaves, Neural Computing and Applications, DOI: 10.1007/s00521-023-09058-y, 2023.

2. Akhiat, Y., Touchanti, K., Zinedine, A. *et al.* IDS-EFS: Ensemble feature selection-based method for intrusion detection system. *Multimed Tools Appl* 83, 12917–12937 (2024). https://doi.org/10.1007/s11042-023-15977-8
3. Ashisha G. R., Anitha Mary X., George T., Martin Sagayam K, Unai Fernandez-Gamiz Hatıra Günerhan, Uddin, M.N. and Pramanik, S. Analysis of Diabetes disease using Machine Learning Techniques: A Review, Journal of Information Technology Management, 2023.
4. Chandan, R. R., Soni, S., Raj, A., Veeraiah, V., Dhabliya, D., Pramanik, S., Gupta, A., Genetic Algorithm and Machine Learning, in "Advanced Bioinspiration Methods for Healthcare Standards, Policies, and Reform", Hadj Ahmed Bouarara, I.G.I. Global, 2023, DOI: 10.4018/978-1-6684-5656-9
5. Haghsheno, H., Arabani, M. Stabilization and solidification of oil-polluted soils using secondary stabilizers and industrial wastes. *Int. J. Environ. Sci. Technol.* 21, 2129–2162 (2024). https://doi.org/10.1007/s13762-023-05285-x
6. Harith, I.K., Abbas, Z.H., Hamzah, M.K. *et al.* Comparison of artificial neural network and hierarchical regression in prediction compressive strength of self-compacting concrete with fly ash. *Innov. Infrastruct. Solut.* 9, 62 (2024). https://doi.org/10.1007/s41062-024-01367-y
7. Khanh, P. T., Ngoc, T. T. H., Pramanik, S., Evaluation of Machine Learning Models for Mapping Soil Salinity in Ben Tre Province, Vietnam, Multimedia Tools and Applications, 2024, https://doi.org/10.1007/s11042-024-18712-z.
8. Le, BA., Tran, BV., Vu, TS. *et al.* Predicting the Compressive Strength of Pervious Cement Concrete based on Fast Genetic Programming Method. *Arab J Sci Eng* 49, 5487–5504 (2024). https://doi.org/10.1007/s13369-023-08396-2
9. Mall, P. K., Pramanik, S., Srivastava, S., Faiz, M., Sriramulu, S. and Kumar, M. N., FuzztNet-Based Modeling Smart Traffic System in Smart Cities Using Deep Learning Models, in Data-Driven Mathematical Modeling in Smart Cities, I.G.I. Global, 2023, DOI: 10.4018/978-1-6684-6408-3.ch005
10. Mondal, D., Ratnaparkhi, A., Deshpande, A., Deshpande, V., Kshirsagar, A. P. and Pramanik, S. Applications, Modern Trends and Challenges of MultiscaleModelling in Smart Cities, in Data-Driven Mathematical Modeling in Smart Cities, I.G.I. Global, 2023, DOI: 10.4018/978-1-6684-6408-3.ch001
11. Sakshi, Bhatia, M.P.S. & Chakraborty, P. Meta-heuristic based feature selection for aberration detection in human activity using smartphone inertial sensors. *Int. j. inf. tecnol.* 16, 559–568 (2024). https://doi.org/10.1007/s41870-023-01484-4
12. Thakur, U., Prajapati, A. & Vidyarthi, A. A bilateral assessment of human activity recognition using grid search based nonlinear multi-task least squares twin support vector machine. *Multimed Tools Appl* (2024). https://doi.org/10.1007/s11042-024-18993-4
13. Veeraiah, V., Dhabliya, D., Dari, S. S., Kumar, J. R. R., Dhabliya, R., Pramanik, S., Gupta, A. The Impact of Data Science and Participated Geographic Metadata on Improving Government Service Deliveries: Prospects and Obstacles, in The Ethical Frontier of A.I. and Data Analysis, pp. 320-342, I.G.I. Global, 2024, DOI: 10.4018/979-8-3693-2964-1.ch020
14. Zhang, H., Gu, X., Zhang, F. *et al.* Development of a radial basis neural network for the prediction of the compressive strength of high-performance concrete. *Multiscale and Multidiscip. Model. Exp. and Des.* **7**, 109–122 (2024).https://doi.org/10.1007/s41939-023-00181-w